Special Issue

Reactivity of Ionic Liquids: Reductive Effect of $[C_4C_1im]BF_4$ to Form Particles of Red Amorphous Selenium and Bi_2Se_3 from Oxide Precursors

Monika Knorr and Peer Schmidt*[a]

Temperature-induced change in reactivity of the frequently used ionic liquid 1-butyl-3-methylimidazolium tetrafluoroborate ($[C_4C_1im]BF_4$) is presented as a prerequisite for the rational screening of reaction courses in material synthesis. $[C_4C_1im]BF_4$ becomes active with oxidic precursor compounds in reduction reaction at $\vartheta \geq 200\,^{\circ}C$, even without the addition of an external reducing agent. The reaction mechanism of forming red amorphous selenium from SeO_2 is investigated as a model system and can be described similarly to the Riley oxidation. The reactive species but-1-ene, which is formed during the decomposition of $[C_4C_1im]BF_4$, reacts with SeO_2 and form but-3-en-2-one, water, and selenium. Elucidation of the mechanism was achieved by thermoanalytical investigations. The monotropic phase transition of selenium was analyzed by the differential scanning calorimetry. Beyond, the suitability of the single source oxide precursor $Bi_2Se_3O_9$ for the synthesis of Bi_2Se_3 particles was confirmed. Identification, characterization of formed solids succeeded by using light microscopy, XRD, SEM, and EDX.

1. Introduction

In recent years, the use of ionic liquids (ILs), which are non-conventional molten salts, has increased significantly in the synthesis of particles of inorganic substances. The characteristics of ILs, such as wide liquid range, low vapor pressure, high charge density, high polarity, supramolecular structure, wide electrochemical window, and high thermal stability are highly beneficial for the synthesis of particles of inorganic materials[1]. Potentially, ILs can perform various functions in inorganic material synthesis: Thus, they act as solvent/stabilizer,[2–8] reactant,[9] template,[10] and precursor[6,10] for the reaction. Synthesis strategies using ILs to generate inorganic particles can be realized by chemical reduction,[2,3,7,8,11,12] electrodeposition,[13] thermal decomposition,[5,14] or induced by microwave heating.[12,15,16]

Indeed, the development of new synthesis approaches most often is related to trial and error practice.[17] However, the process of developing new material syntheses by varying the components and reaction parameters is time-consuming as well as cost-intensive. In most cases, the resulting particles are examined in detail, but the reaction mechanism remains vague. Thus, syntheses with ILs frequently can be described as a "black box".[17] Development and further investigation of rational approaches to design low-temperature materials synthesis by using ILs hence should be forced by reaction mechanism screening.

Methods of thermal analysis prove to be highly appropriate for this purpose, especially when a slightly enhanced temperature is applied. In this respect, the concept of Maximum Operation Temperature (MOT) of ionic liquids comes into focus for the evaluation of thermally induced reactivity of the respective IL.[18–21] This kinetic model makes it possible to determine a temperature at which no more than 1% of the IL has been thermally decomposed within a specified period. If this temperature or the respective time frame is exceeded, a continuous decomposition of the IL occurs. Preliminary work clarifying the decomposition mechanism of some imidazolium-based ionic liquids $[C_2C_1im]X$ (X = Cl, I, Br),[18,19] $[C_4C_1im]X$ (X = Cl, I, Br),[19] and $[C_4C_1im]BF_4$[21] reveal the occurrence of a complex gas-phase already at a rather low temperature when the MOT is reached. The species formed can potentially induce a further reaction of the IL used initially as a solvent. Subsequently, the reactive species can lead to changes in the intended reaction mechanism, and thus to the formation of unexpected reaction products. This study focuses on a model system to evaluate the change in reactivity of ionic liquids while decomposition just starts and to establish the mechanism of the resulting reaction. The ionic liquid 1-butyl-3-methylimidazolium tetrafluoroborate $[C_4C_1im]BF_4$ (or $[BMIM]BF_4$) was used for these exemplary investigations as it is widely used in the low-temperature synthesis of particles of a variety of elements (e.g. Fe, Ag, Ir, Cu, Se, Te).[2,5,7,8,11,15,16] Moreover, ionic liquids containing butyl side chains and BF_4- as anion were successfully applied in materials

[a] M. Knorr, Prof. P. Schmidt
Chair of Inorganic Chemistry
Brandenburg University of Technology (BTU) Cottbus-Senftenberg
Universitätsplatz 1
01968 Senftenberg (Germany)
E-mail: peer.schmidt@b-tu.de

Supporting information for this article is available on the WWW under https://doi.org/10.1002/open.202000264

Special Issue *An invited contribution to a Special Issue dedicated to Material Synthesis in Ionic Liquids.*

syntheses of chalcogens (Te) and chalcogenides (e.g. Bi_2S_3, Bi_2Te_3) by using the oxides and nitrates of the elements as precursors. Generally, these reactions have been realized thermally induced in an oil bath or microwave-assisted.[22,23,24] In these reactions, the oxides were usually reduced to metallic particles by the addition of Sodium tetrahydridoborate ($NaBH_4$).[2,22,25]

In our study, the reaction mechanism of the formation of selenium was analyzed taking SeO_2 and $[C_4C_1im]BF_4$ as starting materials. To date, it has been described that SeO_2 is reduced electrochemically in different ILs.[26] However, our experimental approach is targeted to study the reducing effect of the IL itself.

As a special feature, the application of single-source precursors of Bismuth selenate(IV) ($Bi_2Se_xO_{3+2x}$[27,28]) for the preparation of Bi_2Se_3 is introduced. In particular, our investigations are intended to prove the appropriateness of $Bi_2Se_3O_9$, also referred to as bismuth(III) selenate(IV) - $Bi_2(SeO_3)_3$, as a precursor compound, because of the precast stoichiometric ratio of Bi:Se = 2:3.

Finally, our studies on the reaction mechanism have been realized to promote the rational understanding of the reaction pathways in ILs and to gain findings on the suitability of the selected precursors in the synthesis of chalcogens and chalcogenides, too.

2. Results and Discussion

2.1. Reaction Screening

The investigations of the reduction mechanism of SeO_2 were carried out based on the approach of Zhu *et al.*,[22] who have successfully synthesized tellurium nanorods and nanowires in an IL-based system with TeO_2 as the starting material under the addition of $NaBH_4$ and other additives. Here, it is proposed that $[C_4C_1im]BF_4$ acts similarly for reactions of SeO_2. To uncover the actual function of $[C_4C_1im]BF_4$ thermal screening by differential scanning calorimetry (DSC) has been performed both, under the addition of $NaBH_4$ and without an external reducing agent. (Figure 1).

Preparation of the sample of $[C_4C_1im]BF_4/SeO_2$ with the addition of $NaBH_4$ leads already at ambient temperatures to the very slow reaction of the white powder SeO_2 forming a red precipitate, which subsequently identified by X-ray diffraction and REM/EDX analysis as red amorphous selenium. Thermal screening of the initial mixture (curve 1, Figure 1) proves the start of the exothermic reaction (A1) at $\vartheta_{onset,DSC} = 95\,°C$ ($\vartheta_{peak,DSC} = 105\,°C$). The following exothermic effect was recorded at the temperature of $\vartheta_{onset,DSC} = 150\,°C$ ($\vartheta_{peak,DSC} = 155\,°C$) (A2). Melting of the reduced selenium can be observed at $\vartheta_{onset,DSC} = 220\,°C$ ($\vartheta_{peak,DSC} = 222\,°C$) ($A_3$). Curve 2 (Figure 1) indicates the reaction of the solvent ($[C_4C_1im]BF_4$) with the reducing agent ($NaBH_4$) – but without addition of SeO_2. The resulting exothermic effect at $\vartheta_{onset,DSC} = 140\,°C$ ($\vartheta_{peak,DSC} = 160\,°C$) (B) can be identified by complementary analyses as partial decomposition of IL and formation of $NaBF_4$(s), as proven by pXRD.

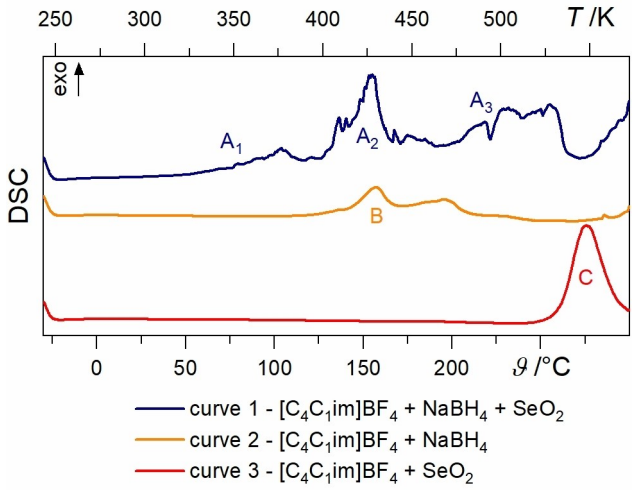

Figure 1. DSC-thermogram of the system $[C_4C_1im]BF_4/SeO_2$ under addition of $NaBH_4$ as a reducing agent (curve 1); comparison of a mixture of $[C_4C_1im]BF_4/NaBH_4$ (curve 2), and $[C_4C_1im]BF_4/SeO_2$ without addition of $NaBH_4$ (curve 3). All measurements are performed with a heating rate of 10 K·min^{-1}.

The reaction pathway was further investigated without the addition of the external reducing agent $NaBH_4$ (curve 3, Figure 1). Here, the reaction screening by DSC shows one exothermic effect at $\vartheta_{onset,DSC} = 262\,°C$ ($\vartheta_{peak,DSC} = 277\,°C$) (C). Optical and X-ray diffraction analysis of the contents of the crucible after the reaction reveal the formation of red amorphous selenium, as well. That is, the exothermic effect at $\vartheta_{onset,DSC} = 262\,°C$ can be assigned to a reduction reaction of SeO_2 inherent in the system. As a first conclusion, the IL itself should act as a reducing agent.

Following, the experiments without the addition of $NaBH_4$ have been reinforced to identify the mechanism of reduction of SeO_2 in $[C_4C_1im]BF_4$ in more detail. Since the reduction takes place at gentle temperatures, it was assumed that not the IL itself but its formed decomposition products can be responsible for the reduction of the oxide. Based on this assumption we come back to the concept of the maximum operation temperature (MOT), which clearly describes the thermal stability of the respective IL and the formation of decomposition products even at moderate temperatures.[18–21]

2.2. Analysis of the Reaction Mechanism

The species responsible for the reduction and the exact reaction mechanism in the $[C_4C_1im]BF_4/SeO_2$ system were investigated and clarified using complementary analytical methods such as dynamic calorimetry (DSC) and thermogravimetry using coupled gas analysis methods (TGA-MS and TGA-FTIR).

First DSC measurement for the mixture $[C_4C_1im]BF_4/SeO_2$ at 10 K·min^{-1} clearly shows the occurrence of an exothermic reduction above 250 °C. However, the influence of the heating rate and thus the length of time the sample was kept at elevated temperatures should be investigated in more detail. Next samples of the reaction system were prepared according

to the description in the experimental section, and corresponding DSC measurements at 5 and 1 K·min^{-1} were performed in a temperature range from −30 °C to 300 °C. The onset temperature decreases steadily to 238 °C as the heating rate is reduced (1 K·min^{-1}, Figure 2).

Obviously, the decomposition temperature range of $[C_4C_1im]BF_4$, described in literature to be between 361 °C and 424 °C,[29] is still far from being reached. Thus, superficially a direct reduction of SeO_2 by $[C_4C_1im]BF_4$ could be assumed. However, previous results show that a significant amount of at least 1.5 % of the IL is already decomposed at temperatures up to 300 °C.[21]

Therefore, to investigate whether the IL itself or the decomposition of the IL is responsible for the observed reduction, the according onset temperatures of different heating rates in the system $[C_4C_1im]BF_4/SeO_2$ were related to the more suitable kinetic model of the MOT, which represents the time-dependent thermal stability of the IL. Accordingly, the MOT describes the period during which the IL should not exceed a certain temperature setpoint; otherwise, more than 1 % is thermally decomposed.

The observed significant shift of the exothermic effect of DSC measurement representing the reduction of SeO_2 (Figure 2) indicates, that the reduction of SeO_2 is not based on a direct reaction with $[C_4C_1im]BF_4$, since otherwise, the onset temperature would remain in a small range, slightly depending on the heating rate. Rather, we can detect a significant dependence on the exposition time at elevated temperature: By reducing the heating rate from 10 K·min^{-1} to 1 K·min^{-1}, the duration of the experiment is extended. Concomitantly, with a longer experiment duration, the temperature indicated by the *MOT decreases*. The shift of the onset temperatures at 10 K·min^{-1} at 262 °C to 238 °C at 1 K·min^{-1} thus can be related to the time-dependent thermal decomposition of $[C_4C_1im]BF_4$.

With this knowledge, further experiments were carried out in vials using aluminum block treatment (see experimental section). Since selenium melts at 220 °C, the temperature for the large batch was confined to 215 °C. After reaching the endset temperature, the sample was held for three hours. Considering the reaction batch that contains only the IL, it becomes clear that at 215 °C the IL is still clear and optically unchanged compared to the room temperature sample, see Figure 3. However, this changes after only one hour at 215 °C. The IL has slightly changed to a cream color. This optical discoloration into orange increases with increasing time (Figure 3). Evidence of decomposition-induced coloration of $[C_4C_1im]BF_4$ can already be found in the literature.[30]

Based on the data of the MOT for $[C_4C_1im]BF_4$[21] a maximum exposition time of about 20 min is calculated at 215 °C – otherwise, decomposition already runs with conversion rate > 1 %. The beginning of the decomposition can be recognized optically by the discoloration after one hour. This increases with increasing time at 215 °C. The time-dependent course of optical discoloration of the IL in the vial and thus the advancing decomposition agrees well with the calculated value of the MOT.

A visual comparison of the reaction mixtures of pure IL with the reaction mixture of $[C_4C_1im]BF_4$ with the addition of SeO_2 shows that the two components do not react at room temperature (Figure 3). The IL is still clear and the white SeO_2 needles are found at the bottom of the vial. If the reaction mixture is heated up to 215 °C, an optical change can already be seen. Above the solid of SeO_2, a slight annular yellow coloration of the IL can be observed. Above this yellow ring, the IL is also slightly cream-colored. This shows that the decomposition of

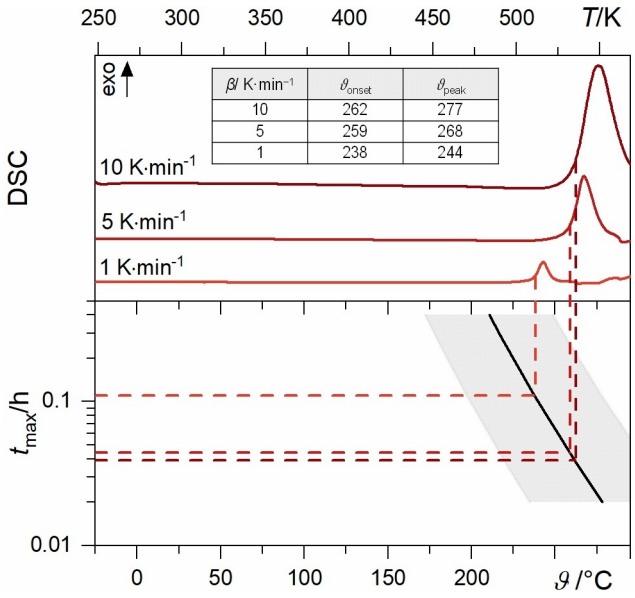

Figure 2. DSC-thermogram of the systems $[C_4C_1im]BF_4/SeO_2$ at different heating rates (1, 5, 10 K·min^{-1}) and calculated MOT range for variable application times.[21]

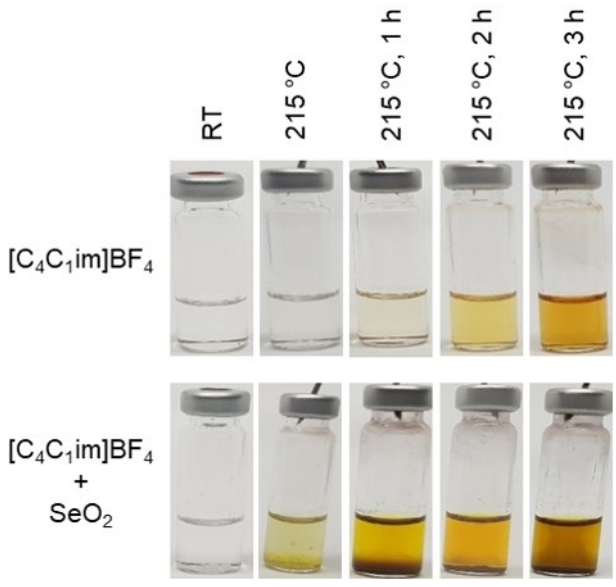

Figure 3. Photo of reaction mixtures $[C_4C_1im]BF_4$ and $[C_4C_1im]BF_4$ with SeO_2 at room temperature (RT), after reaching 215 °C, after a holding time $t = 1$ h, 2 h, 3 h at 215 °C.

the IL and also the reduction of SeO_2 has already occurred when the temperature reaches 215 °C.

The decomposition of the IL has further increased as the reaction time of one hour at 215 °C progresses, which can be seen from the darker color of the IL. Above the SeO_2 at the bottom, a dark red ring-shaped area can be observed. A reaction above the initial solid in the IL can be assumed. After a reaction time of two hours, the ring-shaped area has decreased, thus revealing the complete conversion of the SeO_2 to Se. The formed product mainly sinks to the bottom of the vial, nevertheless, a small amount remains suspended in the liquid. After three hours, the selenium at the bottom of the vial, as well as a further decomposition of the IL, can also be recognized by a more distinct discoloration into brown.

This experimental investigation in vials also shows, complementary to the DSC experiments, that the reduction of SeO_2 to Se can be attributed to a reaction with the decomposition products of $[C_4C_1im]BF_4$. That is, reactive species are formed within the decomposition of the IL, which obviously are responsible for the further reductive effect of $[C_4C_1im]BF_4$.

To obtain more detailed information about the mechanism, it was subsequently investigated whether decomposition products dissolved in IL or gaseous decomposition products are responsible for the reduction of SeO_2 to Se. Further investigations were aimed to elucidate the nature and occurrence of reactive species responsible for the reduction of SeO_2 to Se. For this purpose, a combination of the vial − and DSC experiments were carried out.

At the beginning of the investigation, the clear IL (see Figure 4a) was tempered at 300 °C for 3 h in an aluminum block. Examinations using TGA with a heating rate of 1 K·min^{-1} have already shown a thermal degradation of 1.5 % at 300 °C.[21] Indeed, after a longer application period, the IL is already decomposed to a large extent as shown by the significant brown discoloration of the IL (Figure 4b). The effect becomes reasonable considering the MOT for $[C_4C_1im]BF_4$, which is 174 ± 36 °C for 3 h. Therefore, it can be assumed that sufficient decomposition products have been dissolved in the IL. To test whether the remaining dissolved decomposition products are responsible for the reduction to Se, the former treated sample (300 °C for 3 h) was cooled down to room temperature, the vial's lid was removed and part of the decomposed IL was placed in a new vial in which SeO_2 was already present on the bottom. The absence of a reduction of SeO_2 (Figure 4c) suggests that decomposition products dissolved in the IL are not responsible for the reduction. However, providing activation energy to the system at elevated temperatures could be part of the reactivity. To get insight into reaction actuation, the decomposed sample from (Figure 4b) was placed in a DSC crucible with the addition of SeO_2 and heated again to 300 °C at a heating rate of 1 K·min^{-1}. The screening using DSC with the mixture of decomposed IL and SeO_2 was carried out analogous to the experiment with undecomposed IL (Figure 2). A reduction of SeO_2 can be observed in the same temperature range. (see Supplement, S1) This indicates that the IL is further decomposed and that anew formed gas species become reactive again.

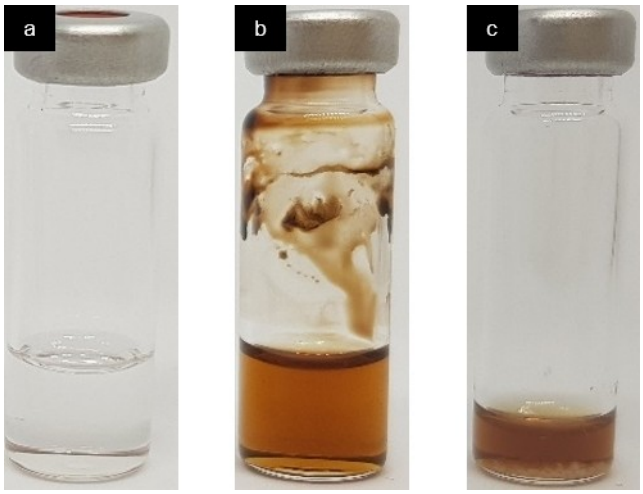

Figure 4. Photo of the reaction batches a) clear $[C_4C_1im]BF_4$ at room temperature, b) decomposed $[C_4C_1im]BF_4$ after a temperature treatment in the Al block at 300 °C for 3 h, c) IL removed after decomposition at 300 °C for 3 h and addition into a vial containing SeO_2.

Based on the strong hints, the reduction of SeO_2 is related to the decomposition of IL, in particular, to the formation of reactive gas species, the subsequent approach has been developed for identification of reactive decomposition gas species by using thermogravimetry with coupled methods of gas analysis. With this respect, mass spectrometry (TGA-MS) was applied initially.

Due to the rather high vapor pressure of selenium even at low temperatures ($p_{300°C} = 5.7 \cdot 10^{-4}$ bar and $p_{500°C} = 0.066$ bar)[31], and to avoid sublimation of Se under the given experimental conditions, MS measurements were confined to a maximum of 300 °C. Otherwise, selenium would be deposited along the transfer capillary, which can only be heated up to a maximum of 300 °C.

With renouncing MS coupling, the thermogravimetric measurements of the system under investigation can be carried out up to 500 °C. Considering the TG or DTG curves with and without SeO_2 (Figure 5a), it becomes clear that with the addition of SeO_2 already at a temperature of $\vartheta_{onset,TG} = 215$ °C ($\vartheta_{onset,DTG} = 217$ °C, $\vartheta_{peak,DTG} = 235$ °C) a mass loss occurs, which is related to the decomposition of $[C_4C_1im]BF_4$ and the reduction of SeO_2. An equilibrium is established between SeO_2 and the formed decomposition products of IL. When the initial amount of SeO_2 is consumed, the curves converge above 300 °C with a slight shift to higher temperatures ($\Delta T_{peak,TG} = 16$ K). However, the decomposition of the IL at higher temperatures cannot be investigated under the addition of SeO_2 using MS with the transfer line.

On closer examination of the fragments detected by MS during IL decomposition and SeO_2 reduction (see Figure 5a), it is possible to assign them to the main species (see Figure 5b) and thus gain insight into the mechanism behind this process.

The evaluation of the detected *m/z*, as well as the assignment to the formed species in the system $[C_4C_1im]BF_4/SeO_2$ was carried out including the known decomposition mechanism of $[C_4C_1im]BF_4$[21], as well as known fragmentation patterns of

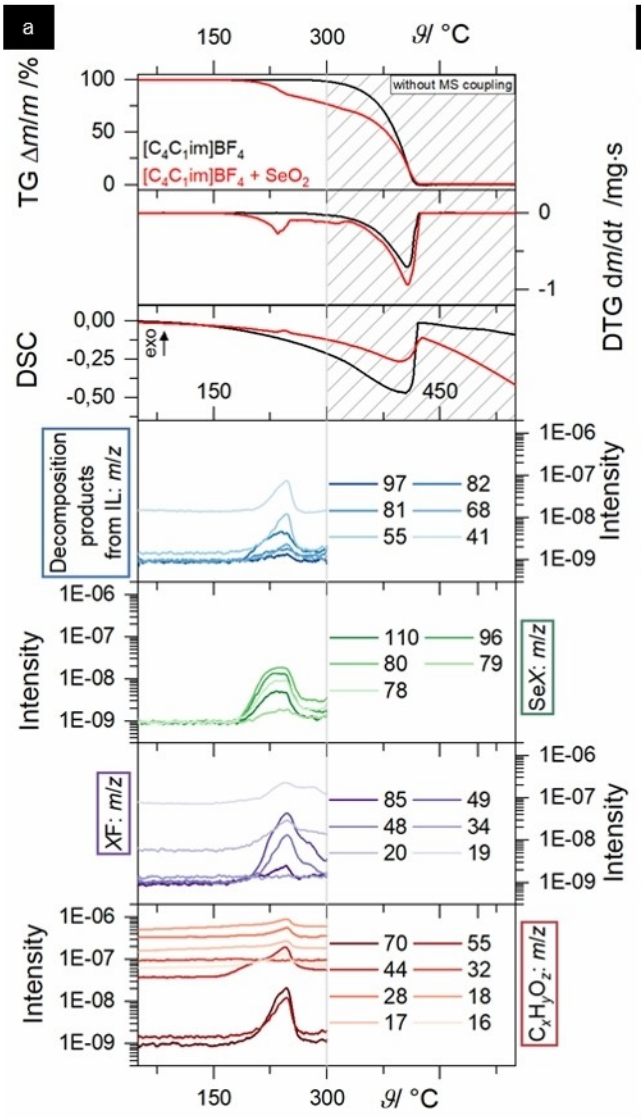

b **list of species**

species	structural detail	resulting *m/z* (>10%)
1−butylimidazole	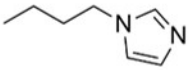	124, 97, 84, **82**, 81, 69, 68, 67, 56, 55, 54, 53, 52, 42, 41, 40, 39, 29, 28, 27
1−methylimodazole	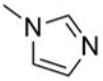	**82**, 81, 55, 54, 42, 41, 40, 28
1 *H*−imidazole	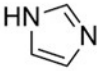	**68**, 41, 40, 28
but−1−ene	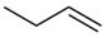	56, 55, **41**, 39, 29, 28, 27, 26
selenium	Se	82, **80**, 78, 77, 76
selenium dioxide	O=Se=O	114, **112**, 110, 109, 108, 98, 96, 94, 80
tetrafluorosilane		**85**
trifluoroborane		**49**, 48
fluoromethane	H_3C-F	**34**, 33, 15
fluorine	F	**19**
fluorane	HF	**20**
water/oxidane	H_2O	**18**, 17
carbon dioxide	O=C=O	**44**, 28, 16, 12
oxygen	O=O	**32**, 16
but−3−en−2−one	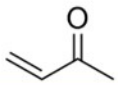	70, **55**, 43, 42, 27, 15

Figure 5. Analysis of the gaseous species by TGA-MS a) TG-, DTG-, DSC-curves of $[C_4C_1im]BF_4$ (black) and $[C_4C_1im]BF_4/SeO_2$ (red), and MS-curves of the main fragments resulting from $[C_4C_1im]BF_4/SeO_2$, b) identified main species and their resulting fragments with characteristic *m/z* (> 10%).

possible decomposition products[32]. The decomposition of $[C_4C_1im]BF_4$ can be described by the S_N2 mechanism with the formation of 1-butylimidazole, trifluoroborane, and fluoromethane or by E2 mechanism with the formation of trifluoroborane, fluorane, 1-methylimidazole, and but-1-ene. Based on the detected *m/z* in the system $[C_4C_1im]BF_4/SeO_2$, it can be assumed that decomposition via the E2 mechanism must be preferred, since there is no increase in the intensity of the *m/z* = 34, which can be assigned to fluoromethane. The formation of 1-butylimidazole can only be confirmed to a limited extent, since *m/z* = 81, 82 were detected, but 1-methylimidazole, which is formed in the E2 mechanism, can also be assigned. The mass number *m/z* = 97, which has the third-highest relative intensity in the fragmentation of 1-butylimidazole, was detected with a slight change in intensity. The fact that trifluoroboranes are formed in both decomposition mechanisms does not allow a statement to be made about the preferred sequence of the E2 mechanism. The characteristic mass number *m/z* = 82 is related to the formation of 1-methylimidazole, while the mass number (*m/z* = 41) is used to prove the decomposition product but-1-ene, formed during the E2 mechanism.

Identification of the *m/z* = 20, which can be assigned to fluoran (HF), deserves closer attention: Former studies on thermal behavior of $[C_4C_1im]BF_4$[21] ascertained occurrence of HF only in the presence of water. This could occur, for example, if the IL used was not dried sufficiently or if the sample was inserted into the STA too slowly. In the present investigation of the system $[C_4C_1im]BF_4/SeO_2$, reliable detection of *m/z* = 20 was possible, additionally to the detection of *m/z* = 18, 17 which shows the presence of water. In this context, a subsequent reaction of fluoran with the silica capillary of the transfer line and the formation of tetrafluorosilane can be recognized by *m/z* = 85.

The statement of HF detection leads to assumption that water must be formed during the reduction of SeO_2. The formation of selenium due to successful reduction of SeO_2 can be shown by identifying the $m/z = 78$, 80 with characteristic isotope pattern of ^{78}Se and ^{80}Se with the ratio of 1 to 2.[33] Small amount of SeO_2 can additionally be detected in the gas phase with similar isotope pattern ($m/z = 110$, 112). Besides the formation of water during the reduction reaction, the release of CO_2 can be possible. Indeed, the occurrence of the fragment $m/z = 44$ can be assigned both to CO_2, C_3H_8 (as a chain fragment), and C_2H_6N (as a ring fragment). Pure oxygen ($m/z = 32$), in contrast, cannot be observed. Finally, the occurrence of mass number $m/z = 70$ gives a strong indication for a special reaction mechanism.

Assuming that $m/z = 70$ is the molecular ion peak and considering the formed decomposition products of IL, a possible assignment as but-3-en-2-one (methyl vinyl ketone) is meaningful. While former investigations on the decomposition mechanism of $[C_4C_1im]BF_4$[21] did not detect this species, its occurrence suggests, that it is associated with the reduction of SeO_2 to Se. As a first result, we succeeded in the identification of decomposition products of the initial mixture $[C_4C_1im]BF_4$/SeO_2 but also gained insight into the reaction mechanism during the reduction of SeO_2 to Se by TGA-MS measurements.

To confirm the results and to obtain further information on the reaction mechanism, a TGA-FTIR measurement was performed in addition to the coupled MS analysis. This allows the identification of atomic groups of the gas species, which are formed during the reaction without being fragmented by high ionization energy during MS.

Both TG and DTG curves of the initial mixture $[C_4C_1im]BF_4$/SeO_2 reveal similar behavior of TGA-FTIR measurement as observed for TGA-MS, too. Thermal degradation runs in a two-step course with characteristic temperature of the first step at $\vartheta_{onset,TG} = 202\,°C$. Due to the characteristic curve shape, the onset of the DTG curve emerges at slightly lower temperature ($\vartheta_{onset,DTG} = 192\,°C$). Furthermore, the respective Gram-Schmidt (G–S) curve covers this behavior with minor shifted temperature course ($\vartheta_{onset,G\text{-}S} = 218\,°C$), caused by the dwell along the transfer capillary. However, the two steps can be assigned again to the reduction of SeO_2 initially, and the subsequent completion of thermal degradation of $[C_4C_1im]BF_4$. The largest mass loss, which is due to the reduction reaction, is observed at $\vartheta_{peak,DTG} = 227\,°C$, and $\vartheta_{onset,G\text{-}S} = 238\,°C$, respectively.

As already shown in the TGA-MS measurement (Figure 5a), the first step is ensued by a plateau of rather flat mass change (Figure 6). The subsequent second step at $\vartheta_{onset,DTG} = 267\,°C$ ($\vartheta_{peak,DTG} = 288\,°C$; $\vartheta_{peak,G\text{-}S} \approx 300\,°C$) can be attributed to the progressive decomposition of $[C_4C_1im]BF_4$. The actual mechanism will be clarified based on the corresponding FTIR spectra. All spectra shown in Figure 6 are presented zoomed in the supplement, S2.

Starting with the onset temperature of DTG curve at $\vartheta_{onset,DTG} = 192\,°C$, the occurrence of characteristic IR signals can be observed, Figure 6. Initially, mainly H_2O and CO_2 are identified in the range from 3500 cm^{-1} to 3050 cm^{-1} and 2400 cm^{-1} to 2250 cm^{-1}, respectively. Indeed a delay is

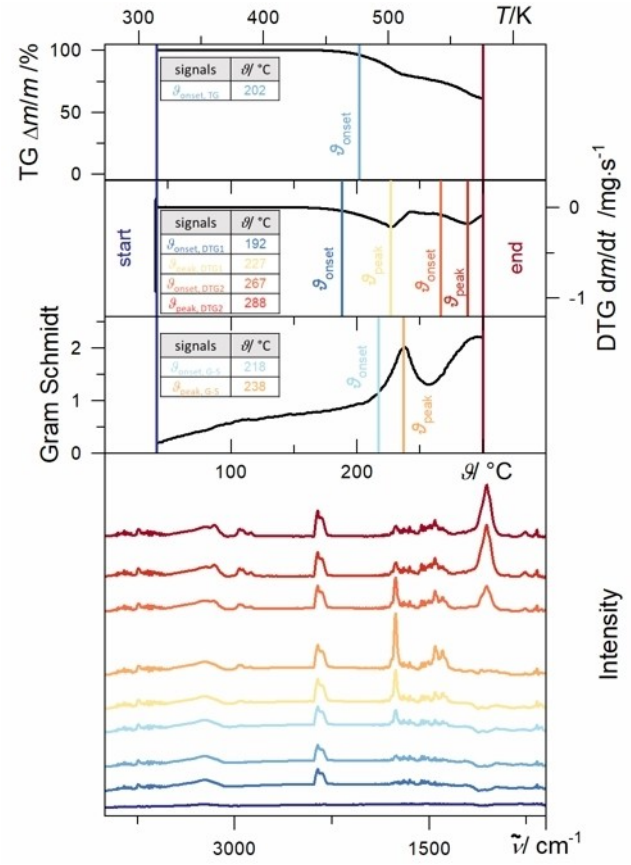

Figure 6. TG-, DTG- and Gram-Schmidt curve for the system $[C_4C_1im]BF_4$/SeO_2 under argon atmosphere with a heating rate of 1 K·min^{-1}, together with IR spectra at characteristic temperatures ϑ_{onset} and ϑ_{peak} of the TG-, DTG- and Gram-Schmidt curve.

observed between the DTG and Gram-Schmidt curve due to the dwell along the transfer capillary, and thus this spectrum can be attributed to the background of the measurement, caused by impurities of the carrier gas (Ar).

Significant changes of the IR signal can be identified in the spectrum at the onset of the Gram-Schmidt curve. The distinctive signal is localized at 1758 cm^{-1}, increasing in intensity with rising temperature until it reaches its highest intensity at the Gram-Schmidt peak ($\vartheta_{peak,G\text{-}S} = 238\,°C$). After that, the intensity of the signal decreases again. Furthermore, two signals can be detected in the range between 1500 cm^{-1} and 1345 cm^{-1}. These signals rise again to $\vartheta_{peak,G\text{-}S} = 238\,°C$, and then decrease in intensity, whereby the signal at 1398 cm^{-1} decreases in intensity much faster than the signal at 1455 cm^{-1}. From $\vartheta_{peak,DTG} = 227\,°C$, three signals in the range between 3000 cm^{-1} and 2820 cm^{-1} can be observed in the shown spectrum. These signals increase in intensity as the temperature rises and remain present over the entire temperature range. The signals in the range between 3000 cm^{-1} and 2820 cm^{-1}, the signal at 1758 cm^{-1}, and both signals in the range between 1500 cm^{-1} and 1345 cm^{-1} are be attributed to the reduction reaction from SeO_2 to Se.

Hereafter, from $\vartheta_{onset,DTG2} = 267\,°C$, altered signals in the FTIR spectrum can be identified, which can be assigned to the

second signal of the DTG curve. The spectrum includes two characteristic signals in the range between 3425 cm^{-1} and 3075 cm^{-1}. Furthermore, a signal which increases in intensity with increasing temperature is formed with a peak at 1058 cm^{-1}. More signals which can be assigned to the second signal of the DTG curve are in the range between 950 cm^{-1} and 700 cm^{-1}. These also increase in intensity with increasing temperature until the end of the measurement at 300 °C.

To identify and to distinguish the formed gaseous reaction products in different steps of the respective TG curve, the spectra at defined temperature of the Gram-Schmidt peak ($\vartheta_{peak,G\text{-}S}$ = 237 °C) and the DTG-Peak 2 ($\vartheta_{peak2,DTG}$ = 288 °C) were compared with reference spectra, Figure 7. Mainly the occurrence of but-3-en-2-one, which was assumed from TGA-MS measurements, should be proven here in detail.

The signal with the highest intensity is located at 1760 cm^{-1} and has a shoulder at 1789 cm^{-1}. These signals generally can be assigned to the carbonyl band. Carbonyl compounds have a very intensive C=O absorption in the range between 1800 cm^{-1} and 1650 cm^{-1}. However, this characteristic stretching vibration of the carbonyl group can be assigned to a large number of carbonyl compounds. A comprehensive discussion of the assignment of the carbonyl band based on band positions compared to the observed band at 1760 cm^{-1} is given in the supplement (S3). Finally, the occurrence of this band for aldehyde, carboxylic acid, acid halide, ester, anhydride, but also amide groups can be excluded.

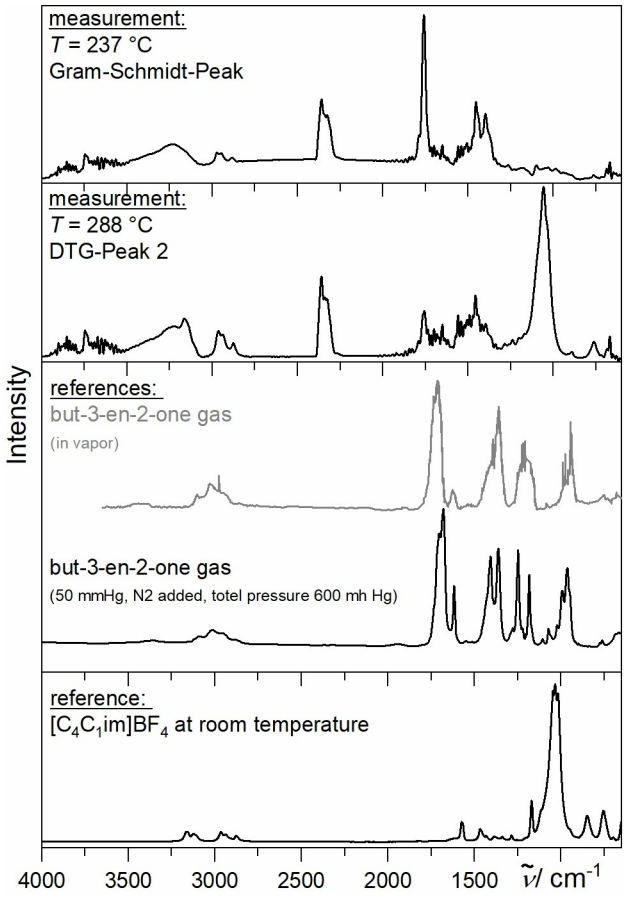

Figure 7. Detailed view of the FTIR-spectra measured at Gram-Schmidt peak ($\vartheta_{peak,G\text{-}S}$ = 237 °C), DTG peak 2 ($\vartheta_{peak2,DTG}$ = 288 °C), as well as reference spectra for but-3-en-2-one which were taken under different conditions[35,37] and reference spectrum of the used IL $[C_4C_1im]BF_4$ at room temperature.[21]

The presence of various formed species in the gas phase and their interaction can serve as an explanation of the significant shift of the C=O stretching vibration towards higher frequencies compared to the usual band position for ketones. Previously, a very complex gas phase could be observed by TGA-MS measurement. Especially fluorine-containing species (BF_3, HF, …), which are present in lower concentrations, can interact with the carbonyl bond and thus enable a high-frequency shift. However, the carbonyl band of but-3-en-2-one appears in the range of 1705 cm^{-1} to 1679 cm^{-1}, depending on the conditions under which the sample is measured. A shoulder can also be observed at 1729 cm^{-1} to 1702 cm^{-1}.[32,34]

The wide band in the range of 3500 cm^{-1} to 3045 cm^{-1} observed in the FTIR spectrum at $\vartheta_{peak,G\text{-}S}$ = 237 °C is related to the stretching vibration of OH and thus H_2O. An additional signal in the range between 2400 cm^{-1} and 2250 cm^{-1} is assigned to CO_2.

The actual origin of both compounds is vague - a simultaneous occurrence from carrier gas and chemical reaction is probable.

Furthermore, three bands (2973 cm^{-1}, 2952 cm^{-1}, 2885 cm^{-1}) can be taken from the spectrum at $\vartheta_{peak,G\text{-}S}$ = 237 °C, which corresponds to the symmetrical and asymmetrical stretching vibration of CH_3. These bands can be assigned in shape and similar position to the butyl group of the IL (see Figure 7), but also to the but-1-ene detected in the decomposition process of $[C_4C_1im]BF_4$.[21] The band position of the three detected bands is similar to the bands in the references for but-3-en-2-one. Band positions for alkenes, which are given in references[32,34], vary widely. In the present measurement, no symmetrical or antisymmetrical stretching vibration for CH_2 can be detected. This could be due to the strong overlay of the broad νOH, but also to the low expression for lower ketones. However, the formation of a double bond can be detected by means of the stretching vibration band of C=C at 1651 cm^{-1}. This can be detected in the references at 1618 cm^{-1} or 1620 cm^{-1}. Another proof for the formation of a double bond, especially a vinyl group, is the intense band at 1453 cm^{-1}, which can be assigned to the deformation vibration of CH. The high intensity can be explained by the fact that the CH group is adjacent to resp. is considered to be a residue of the carbonyl group, thus producing an inducing effect. This intensity amplification can also be applied to the second residue of the carbonyl group of the terminal CH_3 group at 1399 cm^{-1}, which corresponds to the symmetrical deformation vibration of CH_3. These high intensities of both bands can also be observed in references to but-3-en-2-one.[32,34]

Symmetrical and asymmetrical stretching vibration of the skeleton can be detected at 1267 cm^{-1} and 763 cm^{-1}. These correspond to the position in both references, but the intensities of the measured bands are significantly lower compared to those of the references. These low intensities can also be detected at *w*CH_2 (1101 cm^{-1}), *r*CH_3 (1031 cm^{-1}), *t*CH_2

(986 cm^{-1}), and rCH_2 (944 cm^{-1}). A comparison of the band position with the references can be seen in Table 1.

According to the present spectrum at $\vartheta_{peak,G\text{-}S} = 237\,°C$, it can be assumed that the gaseous species with $m/z = 70$, which is formed in the course of the reaction in the system $[C_4C_1im]BF_4/SeO_2$, is a compound with keto group (ν C=O at 1760 cm^{-1}). In the formed species, near the keto group, there is a vinyl group (δ = CH at 1453 cm^{-1}) and a methyl group (δ_s CH_3 at 1399 cm^{-1}). This conclusion can be reached because of the high intensity of both bands. Finally, the formation of but-3-en-2-one during the reduction of SeO_2 to Se can be deduced with high certainty by results of TGA-MS and TGA-FTIR.

The FTIR spectrum was taken at $\vartheta_{peak2,DTG} = 288\,°C$ (see Figure 7) clearly shows changes in the intensity of known bands, but also the formation of new bands. To get an understanding of what happens at this stage of the mass loss in the system $[C_4C_1im]BF_4/SeO_2$, the spectrum was analyzed in detail and compared with the spectrum of pure IL at room temperature (see Table 2).

Superimposed on the wide νOH band, two bands, which can be assigned to the symmetrical and asymmetrical stretching vibration of CH_2, can now be detected. These indicate the presence of double bonds. However, it cannot be determined whether the signals originate from the but-3-en-2-one formed, from the but-1-ene formed within the decomposition, or from the imidazole. The bands associated with the symmetrical and asymmetrical stretching vibration of the alkanes are slightly shifted to lower frequencies compared to the spectrum at $\vartheta_{peak,G\text{-}S} = 237\,°C$. The stretching vibration of the carbonyl band (1757 cm^{-1}, 1700 cm^{-1}) can still be detected, but it has strongly decreased in intensity and has also been shifted to lower frequencies.

An indication for the presence of an imidazole compound is the band at 1559 cm^{-1}, which is typical for ν C=C in aromatic compounds. The band at 1457 cm^{-1}, with its high intensity, indicates a deformation vibration of a compound with the vinyl group, which is further evidence of but-1-ene or but-3-en-2-one. Other vibrations that can be associated with but-1-ene and but-3-en-2-one are the deformation vibration of CH_2 at 890 cm^{-1}, but also ν_sCCC at 761 cm^{-1}. Comparing the signal at 1056 cm^{-1} (νBF, νC–C, νC–H) recorded at $\vartheta_{peak2,DTG} = 288\,°C$, with the reference spectrum of pure IL at room temperature (1045 cm^{-1}), it can be seen, that the intensity and width of the signal are equal. However, the nearby bands of the triplet of high frequency (νBF, νC–C) and low frequency (νBF) of the signal at 1056 cm^{-1} are missing or very weak. For this reason, it cannot be determined whether the stretching vibration of BF can be added to the signal at 1056 cm^{-1}.

Based on the spectrum at $\vartheta_{peak2,DTG} = 288\,°C$, it is possible to make statements about the second DTG mass loss stage of this measurement (Figure 6).

Table 1. Bands of the vibration spectrum at $\vartheta_{peak,G\text{-}S} = 237\,°C$ in the system $[C_4C_1im]BF_4/SeO_2$ and bands for reference spectra for but-3-en-2-one[32,34], which were taken under different conditions.

Vibrational spectra at $\vartheta_{peak,G\text{-}S} = 237\,°C$ $\tilde{\nu}$/cm−1	reference spectra for but-3-en-2-one from NIST[32] $\tilde{\nu}$/cm^{-1}	reference spectra for but-3-en-2-one from Durig *et al.*[34] $\tilde{\nu}$/cm^{-1}	assigments×
3235			ν OH
	3361	3105	νas CH2 (alkene)
	3092	3036	νs CH2 (alkene)
	3012	3019	ν CH
2973	2947	2971	νas CH3 (alkane)
2952		2936	νas CH3 (alkane)
2885	2874		νs CH3 (alkane)
1789	1702	1729	ν C=O
1760	1679	1705	ν C=O
1651	1618	1620	ν C=C
1453	1407	1400	δ = CH (vinyl group)
1399	1363	1366	δs CH3
1267	1248	1218	νas CCC
1101	1184	1062	w CH2
1031		1002	r CH3
986	995	987	t CH2
944	964	950	r CH2
763	762	758	νs CCC

× ν, stretch; δ, bend; w, wagging; t, twisting; r, rocking; γ, out-of-plane; s, symmetrical; as antisymmetrical.

Table 2. Bands of the vibration spectrum at $\vartheta_{peak2,DTG} = 288\,°C$ in the system $[C_4C_1im]BF_4/SeO_2$ and bands for reference spectra for $[C_4C_1im]BF_4$ from Knorr *et al.*[21]

Vibrational spectra at $\vartheta_{peak,DTG} = 288\,°C$ $\tilde{\nu}$/cm^{-1}	reference spectra for $[C_4C_1im]BF_4$ from[21] $\tilde{\nu}$/cm^{-1}	assigments×
3221	3161	νas CH2 (alkene)
3166	3121	νas CH2 (alkene)
2965	2963	νs CH3, νas CH2 (alkane)
2941	2937	νs CH3, νas CH2 (alkane)
2877	2876	νas CH3, νs CH2 (alkane)
1757		ν C=O
1700		ν C=O
1651		ν C=C
1559	1574	ν C=C (aromatic compound)
1492	1466	δas CH3 (Me)
1457	1431	δs CH3 (Me), δ = CH2
1398	1385	δs CH3, w CH2
	1338	ν N–Bu, ν N-Me
1286	1284	ν BF, t CH2
1241	1253	t CH2, r C2-H
1171	1169	ν N–Bu, ν N–Me, r C-H
	1045	ν BF, ν C–C
1056	1033	ν BF, ν C–C, ν C-H
1033 sh	1017	ν BF
890		w CH2, δ CH2 (alkene), ν C-C
	848	γ C4-H, C5-H
761	753	νs CCC

× ν, stretch; δ, bend; w, wagging; t, twisting; r, rocking; γ, out-of-plane; s, symmetrical; as antisymmetrical.

Based on the changes and additional signals in comparison to the spectrum at $\vartheta_{peak,G\text{-}S} = 237\,^{\circ}C$, it can be seen that the reduction of SeO_2 to Se with the formation of but-3-en-2-one must have been almost completed since characteristic bands for but-3-en-2-one have decreased strongly in intensity. Among others, the band at 890 cm^{-1} could confirm the presence of the reductive species but-1-ene in the gas phase. Thus, the but-1-ene formed during the decomposition of $[C_4C_1im]BF_4$ remained in the gas phase after the complete consumption of SeO_2. The methylimidazole also formed during decomposition can be identified in addition to the band with medium intensity at 1559 cm^{-1}.

Based on previous results on the decomposition mechanism of $[C_4C_1im]BF_4$[21] the current results of the TGA-MS- and TGA-FTIR-experiments can be meaningfully combined, and thus the reaction mechanism that leads to the reduction of SeO_2 to Se can be enlightened.

Initially, incipient thermal decomposition of $[C_4C_1im]BF_4$ leads to the formation of but-1-ene during decomposition of $[C_4C_1im]BF_4$ by both S_N2 and E2 mechanism.[21] Similarly, the formation of but-1-ene during the decomposition of other imidazolium-based ionic liquids $[C_4C_1im]X$ (X = Cl, Br, I) is described by Efimova.[19] Further, reaction between but-1-ene and selenium dioxide results in reduction of SeO_2 forming selenium.

The oxidation of the methylene group of but-1-ene finally results in formation of but-3-en-2-one. Our results refer to the reaction mechanism, described by Riley *et al.* as early as 1932 for the oxidation of alkenes by SeO_2 to form allylic alcohols – commonly termed as Riley oxidation.[35] Further studies by Riley showed that in presence of ethylene at elevated temperatures sublimation of SeO_2 furthermore leads to the reaction of gaseous ethylene to glyoxal under the formation of water.[36]

Involving alkenes with longer chains, a keto group is formed in the gas phase.[36,37] However, the reaction mechanism of Riley oxidation with the formation of allylic alcohol was successfully explained by Sharpless *et al.* in 1972.[38] This mechanism is the most widely accepted one. Allylic oxidation by SeO_2 is quite special, as it is one of only a few chemical reactions, in which selective insertion of oxygen occurs, without structural rearrangement of the starting compound.[39] The double bond present in the educt is also retained at the same position in the product.

Finally, the current reaction mechanism of reduction of SeO_2 by $[C_4C_1im]BF_4$ can be described entirely: As a precondition, the thermal degradation of the ionic liquid causes reactive species, when the maximum operation temperature (MOT) is exceeded. Here, most importantly but-1-ene is formed during the decomposition of $[C_4C_1im]BF_4$[21]. Even if but-1-ene is highly volatile and thus mainly identified in the gas phase, the reaction with SeO_2 takes place in the liquid phase – directly at the interface between solid SeO_2 and the IL. This behavior is similar to an Alder-ene reaction from the mechanistic point of view (Scheme 1, step 1) under formation of an allylic selenic acid. In the second step of the mechanism, a [2,3] sigmatropic rearrangement of the allylic selenic acid takes place, forming the intermediate product of the selenium(II) ester. In the third and last step, the metastable intermediate is decomposed, resulting in dehydration and release of the selenium. In the formed product but-3-en-2-one, the double bond is now in its original position as in the educt but-1-ene. Besides, however, an allylic carbonyl compound in the form of a ketone group was introduced at the *C3* position of but-1-ene. This mechanism can be used to explain the local selectivity of the reaction at but-1-ene caused by the ene step, but also the preference of the formation of the allylic ketone group resulting from the [2,3] rearrangement with the formation of reduced selenium and water.

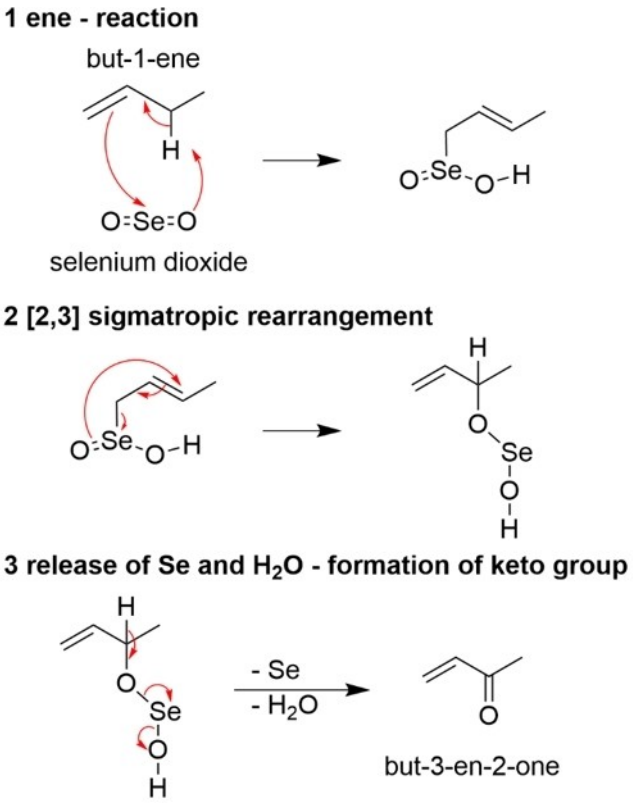

Scheme 1. Reaction mechanism in the system $[C_4C_1im]BF_4/SeO_2$, which leads to the reduction of SeO_2 to Se and the formation of but-3-en-2-one and water.

It is to emphasize, that not the ionic liquid itself becomes reactive, but their incipient decomposition leads to the formation of several reactive gas species. Mainly but-1-ene, which commonly appears during the decomposition of ionic liquids with butyl side chains[19],

is responsible for the reduction of SeO_2 forming Se. Using the complementary analytical methods of TGA-MS and TGA-FTIR, the detection of the educts but-1-ene and SeO_2 in the gaseous phase as well as the identification of the formed products Se, H_2O, and but-3-en-2-one were successful. The product was subsequently characterized in more detail.

2.3. Analysis of the Obtained Solid in the $[C_4C_1im]BF_4/SeO_2$ System

Previously conducted experiments in vials (Figure 3) at 215 °C for $t = 1$, 2, 3 h have shown that the white SeO_2 used is transformed into a red solid. Using TGA-MS the reduction of SeO_2 to Se could be detected. However, since selenium can occur in different allotropes, the solid product formed in the system $[C_4C_1im]BF_4/SeO_2$ was investigated in more detail. For this purpose, the precipitated solid was isolated and dried under dynamic vacuum ($1.0 \cdot 10^{-3}$ mbar). A red powder could be seen under the light microscope (Figure 8a). An investigation using pXRD (Figure 8b) revealed the solid to be completely amorphous, since no reflections could be detected in the diffractogram. Clearly, no reflexes of the educt SeO_2 could be observed in addition (Figure 8b).

For imaging the surface and determining the size of the particles of red amorphous selenium that were obtained, investigations were carried out using a scanning electron microscope. Figure 8c shows irregular areas, which can be attributed to the amorphous selenium, but also spherical inclusions in the irregular areas. A determination of the chemical composition of both, the irregular regions and the spherical inclusions, using EDX (Figure 8d) showed that both are solely composed of selenium. Obviously, the spherical particles, which could have a diameter of up to 20 µm, have been formed from molten areas, when the synthesis temperature achieved close to the melting point of 220 °C.

After a short time observing the sample under the light microscope some areas of the red amorphous selenium transformed into shiny grey particles, see Figure 8e. As time passed these areas increased under the light microscope until the transformation was complete. After conversion, formation of the stable grey hexagonal selenium modification was confirmed by pXRD (Figure 8f). This phenomenon was already described in 1970 by Gobrecht *et al.*[40].

The further prove of phase formation pathway succeeded by DSC measurement of initial sample of red amorphous selenium, which was heated to 300 °C at a defined heating rate of 1 K·min^{-1}, Figure 9. Quite obviously, a monotropic phase transition with exothermic effect at a temperature of 88 °C and endothermic melting at 220 °C is observed. However, the curve is to evaluate in more detail, thus emphasizing a very small endothermic effect (A) ($\vartheta_{onset,DSC} = 47$ °C). The peak characteristic let us generally assume a glass transition. Otherwise, different references describe the occurrence of phase transition from the red allotrope into the black amorphous modification with changing temperatures (30 °C or range of 37 ± 10 °C).[40,41] At the onset temperature of 88 °C the cold crystallization (B) takes place, which corresponds to a transition into the crystalline sample of hexagonal grey allotrope (s.g. P3121[42]). Coinciding, temperatures of 80 °C[40] and 81 °C,[43] but also ranges of 113 °C to 124 °C[44] are given in the literature for crystallization of selenium in the thermodynamic stable modification. Such a spread temperature range is typical for monotropic phase transition, which is induced by thermal activation under slightly different experimental conditions.

The large endothermic effect (C) ($\vartheta_{onset,DSC} = 220$ °C) can finally be assigned to the melting of crystalline hexagonal selenium. No crystallization can be observed in the cooling curve, Figure 9. Rapid cooling with a rate of 10 K·min^{-1} leads to the solidification of the black amorphous modification and not

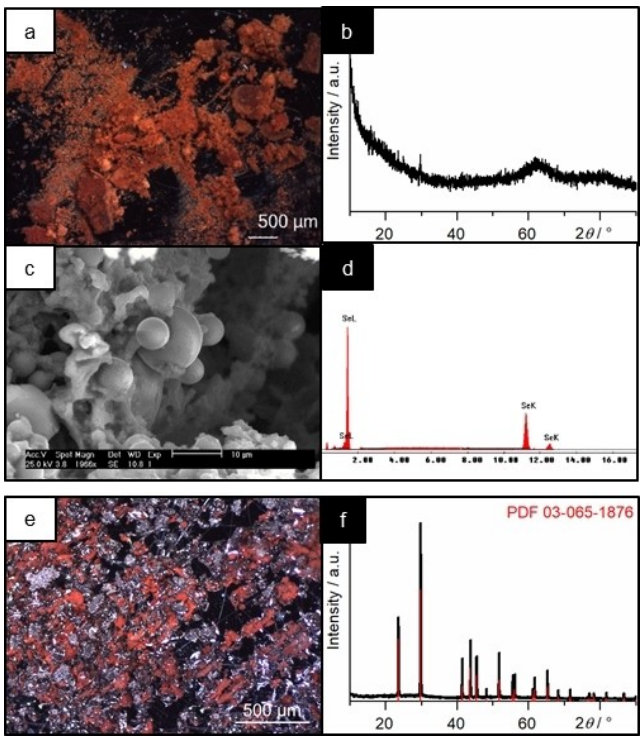

Figure 8. Optical and analytical investigations in the system $[C_4C_1im]BF_4/SeO_2$. a) Light-microscope image of isolated red solid. b) XRD pattern of the amorphous solid (selenium). c) SEM image of irregular regions with embedded spherical particles of amorphous selenium, and d) its EDX spectrum. e) Light microscopic image of the isolated red solid after photo-induced modification and monotropic phase transition into the stable grey modification. f) XRD pattern of the grey modification of selenium (PDF 03-065-1876).

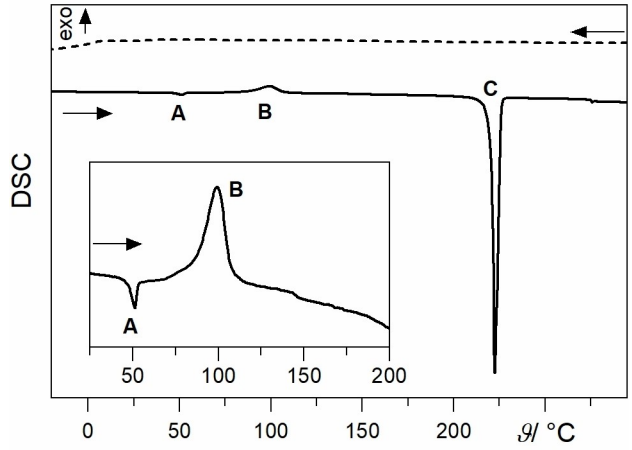

Figure 9. DSC-thermogram of red amorphous selenium with a heating and cooling rate of 10 K·min^{-1}.

to the formation of the crystalline modification[44], therefore no crystallization effect can be observed.

2.4. Synthesis and Analysis of Solids in the System $[C_4C_1im]BF_4/Bi_2Se_3O_9$

The knowledge gained about the reaction mechanism in the system $[C_4C_1im]BF_4/SeO_2$ and the subsequent closer characterization of amorphous selenium will be used to clarify whether, analogous to the reduction of SeO_2 to Se, the oxidic precursor $Bi_2Se_3O_9$ is reduced to Bi_2Se_3. The compound Bi_2Se_3 is aimed at, because similar to Bi_2Te_3, it acts as a promising topological insulator and thermoelectric material for use in electronics.[45] As a possible oxidic precursor in the system Bi_2O_3-SeO_2, six stable phases occur. Since the $Bi_2Se_3O_9$ phase already contains bismuth and selenium in the desired stoichiometric ratio of 2:3 of the target compound Bi_2Se_3, it was considered particularly suitable and the system $[C_4C_1im]BF_4/Bi_2Se_3O_9$ was subsequently investigated in more detail. The synthesis of $Bi_2Se_3O_9$ was carried out as published by Oppermann *et al.*[28] The obtained product was examined for phase purity by pXRD. To understand the course of the reaction, a TGA experiment with the oxidic precursor $Bi_2Se_3O_9$ and $[C_4C_1im]BF_4$ was performed and the obtained curve was compared with measured curves of the systems $[C_4C_1im]BF_4/SeO_2$, $[C_4C_1im]BF_4/Bi_2O_3$, but also the system $[C_4C_1im]BF_4$ with a mixture of Bi_2O_3 and SeO_2 in a ratio of 1:3.

The obtained TG and DTG curves are shown in Figure 10. Up to 150 °C all TG curves are linear. Depending on the sample composition, two to four steps can be identified subsequently. Based on the DTG curves, the individual steps can be precisely assigned. In the system $[C_4C_1im]BF_4/SeO_2$ at $\vartheta_{onset,DTG} = 185$ °C ($\vartheta_{onset,TG} = 194$ °C, $\vartheta_{peak,DTG} = 228$ °C) a loss of mass can be detected, which is due to the reduction of SeO_2 to Se. At $\vartheta_{onset,DTG} = 334$ °C the subsequent decomposition of remaining ionic liquid $[C_4C_1im]BF_4$ occurs. The similar course of the curve and the formation of two stages can also be seen in the $[C_4C_1im]BF_4/Bi_2O_3$ system. The signal of the DTG curve, which is due to the reduction of Bi_2O_3, shifts to higher temperatures to $\vartheta_{onset,DTG} = 230$ °C ($\vartheta_{onset,TG} = 230$ °C, $\vartheta_{peak,DTG} = 251$ °C). The subsequent decomposition of IL is in a similar range as in the system $[C_4C_1im]BF_4/SeO_2$ ($\vartheta_{onset,DTG} = 329$ °C, $\vartheta_{peak,DTG} = 403$ °C).

To analyze whether the compound $Bi_2Se_3O_9$ must be submitted for the targeted synthesis of Bi_2Se_3 or whether a homogeneous mixture of Bi_2O_3 and SeO_2 in a ratio of 1:3 is sufficient as the initial mixture, this was also examined using TGA. In the DTG curve of the mixture of SeO_2 and Bi_2O_3 three signals can be observed, which are due to the reduction of the oxidic starting materials.

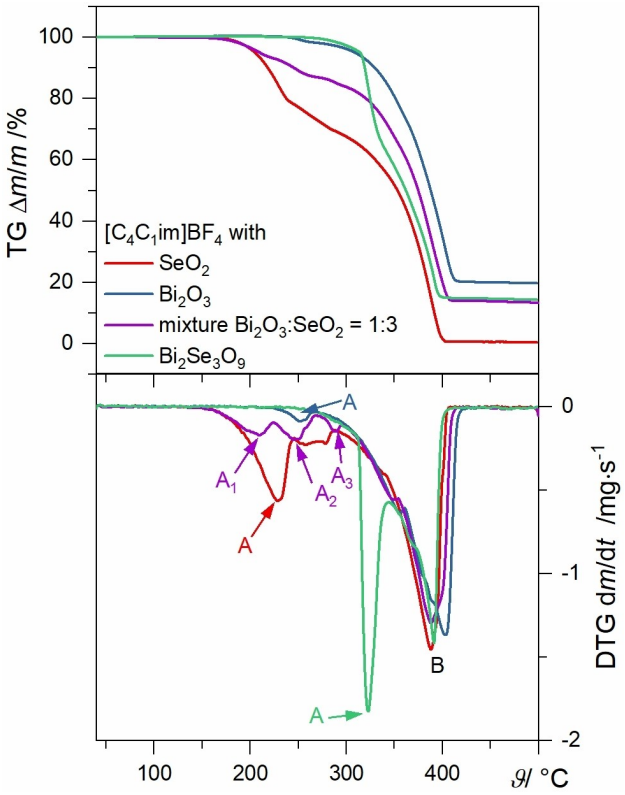

Figure 10. TG and DTG curves of the systems $[C_4C_1im]BF_4/SeO_2$, $[C_4C_1im]BF_4/Bi_2O_3$, $[C_4C_1im]BF_4$/mixture Bi_2O_3:SeO_2 = 1:3 and $[C_4C_1im]BF_4/Bi_2Se_3O_9$ under helium atmosphere with a heating rate of 1 K·min^{-1}.

Based on these signals it can be assumed that SeO_2 and Bi_2O_3 are reduced independently. Based on the DTG curve, a similar curve of the first stage, see Figure 10 signal A_1 can be seen, compared to the first stage in the system $[C_4C_1im]BF_4/SeO_2$. Using the mixture of Bi_2O_3 and SeO_2 in a ratio of 1:3, however, this mass stage is significantly lower. In the second stage, signal A_2, in the system $[C_4C_1im]BF_4/(Bi_2O_3 + SeO_2)$ can be assigned to the reduction of Bi_2O_3, since again the curve is similar to the reduction signal in the system $[C_4C_1im]BF_4/Bi_2O_3$.

Table 3. Determined onset and peak temperatures in the systems $[C_4C_1im]BF_4/SeO_2$, $[C_4C_1im]BF_4/Bi_2O_3$, $[C_4C_1im]BF_4$/mixture Bi_2O_3:SeO_2 = 1:3 and $[C_4C_1im]BF_4/Bi_2Se_3O_9$ from.[21]

			$[C_4C_1im]BF_4/SeO_2$	$[C_4C_1im]BF_4/Bi_2O_3$	$[C_4C_1im]BF_4/(Bi_2O_3 + SeO_2)$	$[C_4C_1im]BF_4/Bi_2Se_3O_9$
reduction of the oxide	A/A_1	$\vartheta_{onset,TG}$/°C	194	230	180	314
		$\vartheta_{onset,DTG}$/°C	185	230	167	313
		$\vartheta_{peak,DTG}$/°C	228	251	209	323
	A_2	$\vartheta_{onset,DTG}$/°C			206	
		$\vartheta_{peak,DTG}$/°C			245	
	A_3	$\vartheta_{onset,DTG}$/°C			269	
		$\vartheta_{peak,DTG}$/°C			289	
decomposition of $[C_4C_1im]BF_4$	B	$\vartheta_{onset,DTG}$/°C	334	329	337	350
		$\vartheta_{peak,DTG}$/°C	388	403	388	391

The mass loss in the third stage (signal A_3) in the system $[C_4C_1im]BF_4/(Bi_2O_3 + SeO_2)$, which is significantly lower than stage one and two, cannot be explained at this point. However, this could be the evaporation of the reduced selenium. Also in this system, a subsequent reduction of $[C_4C_1im]BF_4$ can be detected at $\vartheta_{onset,DTG} = 337\,°C$ ($\vartheta_{peak,DTG} = 388\,°C$). The decomposition of the IL is thus again in a similar range.

The DTG curve of the system $[C_4C_1im]BF_4/Bi_2Se_3O_9$ shows, compared to the system $[C_4C_1im]BF_4/(Bi_2O_3 + SeO_2)$, only one step of the mass loss ($\vartheta_{onset,DTG} = 313\,°C$, $\vartheta_{onset,TG} = 314\,°C$, $\vartheta_{peak,DTG} = 323\,°C$), which is due to the reduction reaction. The reduction of SeO_2 and Bi_2O_3 does not occur independently, similar to the curve in the system $[C_4C_1im]BF_4/(Bi_2O_3 + SeO_2)$, but rather as a simultaneous reduction of Bi_2O_3 and SeO_2. Since the stability of the compound $Bi_2Se_3O_9$ is much higher than the stability of the starting compounds SeO_2 and Bi_2O_3, the temperature to be applied for reduction is shifted to higher values. Also in this system, the decomposition of the IL ($\vartheta_{onset,DTG} = 350\,°C$, $\vartheta_{peak,DTG} = 391\,°C$) can be observed similar to the other investigated systems. Based on the series of experiments of the systems $[C_4C_1im]BF_4/SeO_2$, $[C_4C_1im]BF_4/Bi_2O_3$, $[C_4C_1im]BF_4$/mixture $Bi_2O_3:SeO_2 = 1:3$ and $[C_4C_1im]BF_4/Bi_2Se_3O_9$ it could be shown that the use of a homogeneous mixture $Bi_2O_3:SeO_2 = 1:3$ is unsuitable for the synthesis of Bi_2Se_3 since both components are reduced independently at different temperatures. An investigation of the crucible residue by pXRD also showed that no formation of Bi_2Se_3 occurred during the reaction. Otherwise, using the oxide precursor $Bi_2Se_3O_9$ a single step reduction and thus no preferential extraction of a component is observed.

To determine the optimum reaction conditions, DSC experiments were carried out in the system $[C_4C_1im]BF_4/Bi_2Se_3O_9$ at different heating rates. Figure 11 shows that the reduction of $Bi_2Se_3O_9$ proceeds as an exothermic reaction. Similar to the system $C_4C_1im]BF_4/SeO_2$ (see Figure 2), a shift of the exothermic signal to higher temperatures can be observed by increasing the heating rate. This fact can again be related to the time-dependent thermal stability – the MOT. The use of low heating rates is more likely to cause decomposition of $[C_4C_1im]BF_4$ than the use of higher heating rates and thus the formation of the relevant reactive species which must be responsible for the reduction of the oxide precursor. Comparing the determined onset temperatures at a heating rate of 1 K·min^{-1} in the systems $[C_4C_1im]BF_4/SeO_2$ and $[C_4C_1im]BF_4/Bi_2Se_3O_9$, a clear increase of the onset temperature from $\vartheta_{onset,DSC(SeO2)} = 238\,°C$ to $\vartheta_{onset,DSC(Bi2Se3O9)} = 278\,°C$ can be seen. This observation could already be made in the TGA investigations and is confirmed by the DSC experiments. Based on the onset temperature determined at 1 K·min^{-1} an optimum reaction temperature of 280 °C is determined.

The optimum reaction temperature determined in this way was subsequently applied to syntheses in vials in a heated aluminum block. For visual observation of the reaction process, the appearance of the system $[C_4C_1im]BF_4/Bi_2Se_3O_9$ was documented by a photo before starting the reaction, when the reaction temperature of 280 °C was reached and subsequently after every hour until the end of the experiment after three hours. In addition to the system $[C_4C_1im]BF_4/Bi_2Se_3O_9$, a system without $Bi_2Se_3O_9$ was also investigated simultaneously. This allowed conclusions about the decomposition process of the pure IL, but also conclusions about the optical effect of the addition of the oxidic precursor during the experiment. The photographs of the IL and the system $[C_4C_1im]BF_4/Bi_2Se_3O_9$ taken during the reaction are shown in Figure 12.

This shows that after the addition of $Bi_2Se_3O_9$ to $[C_4C_1im]BF_4$ no reaction at room temperature can be observed. The white solid remains unchanged at the bottom of the vial. The used IL is clear at the beginning of the reaction both without and with $Bi_2Se_3O_9$. If the two vials are subsequently heated to 280 °C, a discoloration to cream color can already be observed in the pure IL. This makes it clear that the decomposition of the IL has already begun and progressed. The observation of the discoloration of the IL and the associated decomposition, already at 280 °C, is confirmed by the calculated values of the MOT.[21] As

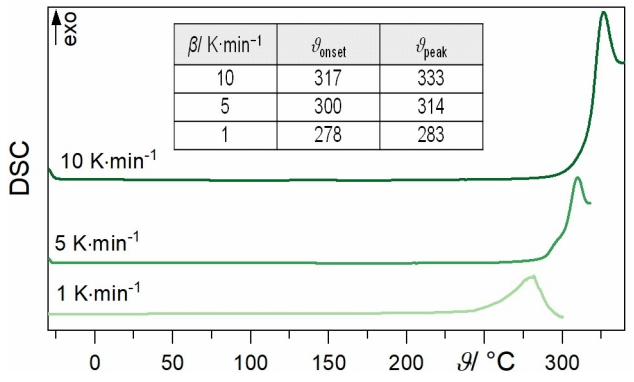

Figure 11. DSC-thermogram of the system $[C_4C_1im]BF_4/Bi_2Se_3O_9$ at different heating rates (1, 5, 10 K·min^{-1}).

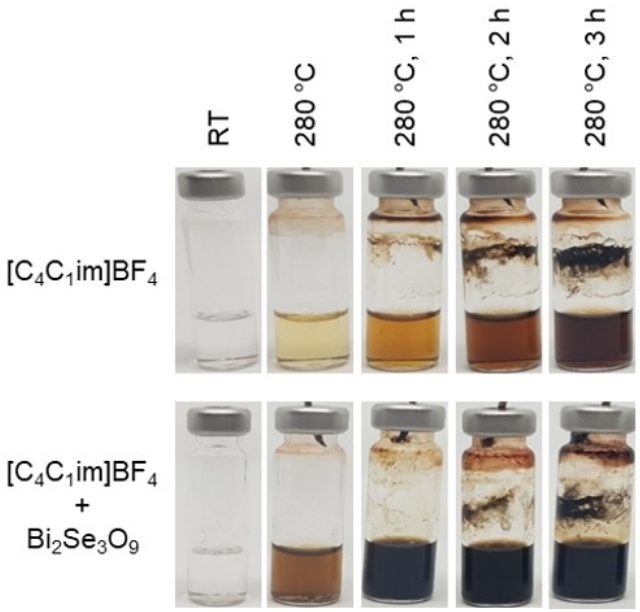

Figure 12. Photo of reaction mixtures $[C_4C_1im]BF_4$ and $[C_4C_1im]BF_4$ with $Bi_2Se_3O_9$ at room temperature (RT), after reaching 280 °C, after a holding time $t = 1$ h, 2 h, 3 h at 280 °C.

the vial with $[C_4C_1im]BF_4$ remains in the aluminum block at 280 °C, the further progress of decomposition and the associated discoloration of the IL from cream to orange to dark brown can be observed. The discoloration respectively decomposition is more advanced than in the analogous experiment, which was performed at a temperature of 215 °C (see Figure 3). This also confirms that the thermal stability of the IL is not only dependent on temperature, but also on the time, the IL is exposed to this temperature. For this reason, in addition to determining the optimal reaction temperature using DSC, the MOT of the IL used should also be calculated before the synthesis and integrated into the reaction planning.

Comparing the appearance of the sample $[C_4C_1im]BF_4$/$Bi_2Se_3O_9$ with the one without $Bi_2Se_3O_9$ after reaching the reaction temperature of 280 °C, it becomes clear that the IL is already discolored significantly darker, which shows that the decomposition is much more advanced than without $Bi_2Se_3O_9$. Small shiny particles can be seen in the brown-colored IL. These were documented by microscopic imaging and are shown in Figure 13a.

Additionally, spots of black coloration can also be seen on the surface of the white solid at the bottom. This fact and the presence of the shiny particles shows that part of the $Bi_2Se_3O_9$ has already reacted. After one hour at 280 °C, the IL of the sample $[C_4C_1im]BF_4$/$Bi_2Se_3O_9$ has turned black. Due to the strong coloration, no more soil particles can be seen. After three hours, the vial with the starting mixture $[C_4C_1im]BF_4$/$Bi_2Se_3O_9$ was removed from the Al-block. A dark precipitate and no more white solid could be detected at the bottom of the vial. Thus, the reaction of the oxidic precursor is finished from optical point of view. The obtained solid was subsequently isolated and dried under dynamic vacuum ($1.0 \cdot 10^{-3}$ mbar).

Investigations of the obtained solid with a light microscope, using a light background (Figure 13b), showed that metallic shining particles, but also small amounts of black particles were formed. These could be small amounts of reduced bismuth. An examination of the obtained solid using pXRD clearly shows that Bi_2Se_3 could be successfully synthesized. However, Bi_2O_3 (PDF 01-079-6679) could be detected as an impurity. The occurrence of Bi_2O_3, which does not have the diffraction pattern of the starting material of Bi_2O_3 (PDF 01-070-8243) used for the synthesis of the precursor, can be explained by the oxidation of unreacted amorphous bismuth. The fact that amorphous bismuth is still present after the reaction can also be recognized by the underground noise, see Figure 13c. The small amount of remaining amorphous bismuth was superficially oxidized during the drying process. However, the existing surface oxide layer can be removed by treatment with diluted HCl. The obtained solid emerges as phase pure Bi_2Se_3, Figure 13c. Thus, the targeted synthesis of Bi_2Se_3 from the oxide precursor $Bi_2Se_3O_9$ in $[C_4C_1im]BF_4$ was successful without the addition of further additives. The amorphous bismuth, which is also still present in small quantities, could probably be removed by adjusting the reaction time. To visualize the obtained particles even more precisely and to check their composition for investigations, they were further characterized by SEM and EDX. Using SEM it was possible to analyze the superficial appearance of the particles more closely. Very thin sheets of Bi_2Se_3 could be observed (Figure 13d). Due to the centrifugation during the isolation of the solid, many of these thin sheets were probably assembled to agglomerations. The agglomerations of the thin sheets, which are only a few nanometers thick, are arranged like petals. This agglomeration in the form of petals is already known from the literature.[24]

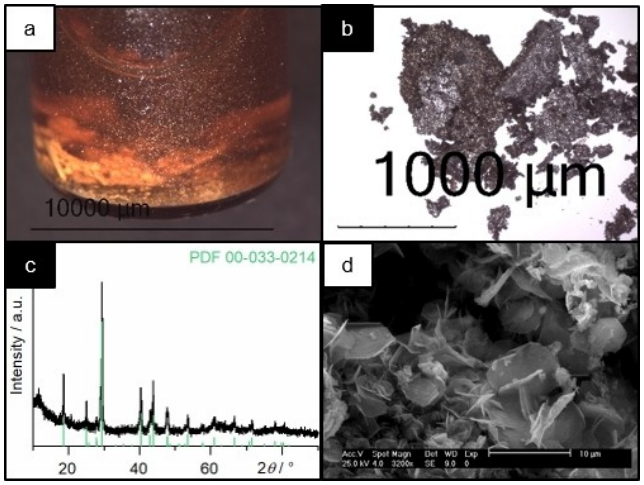

Figure 13. Optical and analytical investigations in the system $[C_4C_1im]BF_4$/$Bi_2Se_3O_9$ a) light-microscope image of the vial after reaching the reaction temperature of 280 °C, b) light-microscope image of the obtained dried solid c) XRD pattern of Bi_2Se_3 (compared to Bi_2Se_3-paraguanajuatite, PDF 00–033-0214), d) SEM image of obtained dried solid showing hexagonal plate crystals of few microns.

The sporadic occurrence of amorphous bismuth, which can be recognized by the irregular particles, can be seen in Figure 13d. An examination of the hexagonal thin sheets for their composition using EDX showed that bismuth and selenium were present in an atomic percentage ratio of 2:3 thus confirming formation of Bi_2Se_3.

As a result, it could be shown using complementary analytical methods that the target phase Bi_2Se_3 has been successfully synthesized at a reaction temperature of 280 °C and a reaction time of 3 h. This was achieved without adding additives to the reaction mixture $[C_4C_1im]BF_4$/$Bi_2Se_3O_9$. The single source oxide precursor $Bi_2Se_3O_9$, in which a Bi:Se ratio of 2:3 is already present, is, therefore, highly suitable for the synthesis of Bi_2Se_3. The prediction of the optimum synthesis temperature based on DSC measurements and inclusion of the MOT for $[C_4C_1im]BF_4$ is thus purposeful.

3. Conclusions

Based on the concept of maximum operation temperature (MOT), the time-dependent thermal decomposition of ionic liquids can be predicted. Exceeding this range, the reactivity of 1-butyl-3-methylimidazolium tetrafluoroborate $[C_4C_1im]BF_4$ significantly changes, and the ionic liquid becomes active with oxidic precursor compounds in reduction reaction at $\vartheta \geq 200$ °C, even without the addition of an external reducing agent.

Using the model system $[C_4C_1im]BF_4/SeO_2$, it could be shown that SeO_2 is reduced to Se with increasing temperature above $\vartheta = 215\,^{\circ}C$ as a result of the formation of reactive gaseous decomposition products of $[C_4C_1im]BF_4$. The thermal decomposition products of $[C_4C_1im]BF_4$ (trifluoroborane, fluorane, 1-methylimidazole, and but-1-ene), which are formed in the course of the E2-mechanism, but also the formation of 1-butylimidazole from the S_N2 mechanism, have been achieved by TGA-MS. The additional occurrence of Se and H_2O, as well as but-3-en-2-one ($m/z = 70$), could be assigned to the reduction reaction. TGA-FTIR measurements finally confirmed the presence of but-3-en-2-one in the formed gas phase. The reaction mechanism leading to the reduction of SeO_2 forming Se thus is identified to be similar to Riley oxidation. The reaction proceeds in three steps as ene-reaction, [2,3] sigmatropic rearrangement, the release of Se and H_2O, and finally the formation of the keto group.

The red powdery solid formed was dried, analyzed by pXRD and SEM, and identified as red amorphous selenium. By DSC measurements, the monotropic phase transitions of selenium from the red amorphous phase to black amorphous selenium ($\vartheta_{onset} = 47\,^{\circ}C$), as well as further transformation into the hexagonal grey modification at $\vartheta_{onset} = 88\,^{\circ}C$ were achieved.

As a special feature, the application of the oxidic single-source precursor $Bi_2Se_3O_9$ was shown to be suitable for the synthesis of Bi_2Se_3 because of the precast stoichiometric ratio of $Bi:Se = 2:3$. The reduction is carried out without the addition of an external reducing agent, too. Optimum synthesis conditions were ascertained to be at least $\vartheta = 280\,^{\circ}C$. Hexagonal thin sheets of Bi_2Se_3 in the dimension of few microns could be characterized in more detail using light microscopy, pXRD, SEM, and EDX.

Experimental Section

Starting Materials/Synthesis of the Oxide Precursor $Bi_2Se_3O_9$

In all experiments, the ionic liquid (IL) 1-butyl-3 methylimidazolium tetrafluoridoborate ($[C_4C_1im]BF_4$) from the company IoLiTec with a purity of 99.5% was used. Before use, it was dried at 80 °C for a period of 6 h under dynamic vacuum ($1.0 \cdot 10^{-3}$ mbar). Selenium dioxide from the manufacturer Sigma-Aldrich, $\geq 99.9\%$ were dried at 70 °C for 12 h. For the synthesis of the oxide precursor $Bi_2Se_3O_9$, bismuth trioxide of the company Aldrich with a purity of 99.9% and selenium dioxide in the stoichiometric ratio $Bi_2O_3:SeO_2 = 1:3$ was weighed in, mixed with mortar, placed in a silica glass ampoule and sealed with an oxyhydrogen gas burner under dynamic vacuum ($1.0 \cdot 10^{-3}$ mbar). The ampoule was tempered as described by Oppermann *et al.*[28] at 250 °C for three days and subsequently at 350 °C for 14 d in a muffle furnace. Afterward, the ampoule was opened, the contained solid was pulverized and examined for phase purity using pXRD. The powder obtained was identified as phase-pure $Bi_2Se_3O_9$. Finally, all substances or samples used were stored and weighed in an argon-filled glovebox LABstar from the manufacturer MBraun ($p(O_2)/p^0 < 1$ ppm, $p(H_2O)/p^0 < 1$ ppm).

Experiments on Thermal Treatment

25 mg of the respective oxidic precursor and/or 900 mg $[C_4C_1im]BF_4$ were placed in a glass vial and capped with a metal lid. To temper the samples, they were placed in an aluminum block, which is heated by a heating plate. The construction used is already described[21]. The experimental setup was located in a fume hood for all experiments. The aluminum block was heated in a range from room temperature to 215 °C, and 280 °C, respectively, and held for a defined time when the target temperature was reached. To remove the gaseous reaction products and at the same time to avoid contact with the air humidity and oxygen, a syringe similar to a drying tube was inserted into the septum of the lid. After a reaction time of 3 h, the obtained solid in the vials was isolated. This was done by repeated washing with dried ethanol and subsequent centrifugation. Following this, the obtained solid was dried under dynamic vacuum ($1.0 \cdot 10^{-3}$ mbar) and further analyzed.

Thermal Analysis

Differential Scanning Calorimetry (DSC)

All experiments were performed with a DSC 1/500 from Mettler Toledo. The measuring range was set to be between −30 °C and 400 °C. Experiments with SeO_2 were performed in 100 µl aluminum crucibles. All experiments with $Bi_2Se_3O_9$ were carried out in 85 µl platinum crucibles, as otherwise, reaction with the standard Al crucible material occurred. All measurements were performed with perforated lids. Heating rates of mostly 1 K·min^{-1}, but also 5 K·min^{-1} and 10 K·min^{-1} and a gas flow of 20 mL·min^{-1} nitrogen were used. Sample masses were 26 ± 2 mg for $[C_4C_1im]BF_4$ and 6 ± 1 mg for SeO_2 and 3 ± 1 mg for $Bi_2Se_3O_9$. The measurement evaluation was done with implemented STAR software (Mettler Toledo). For each thermal effect, the characteristic temperatures were evaluated both at the onset (ϑ_{onset}) and the peak (ϑ_{peak}). The characteristic heat flow – and thus the enthalpy direction – of the thermal effects was indicated in each figure (up = exothermic, down = endothermic).

Simultaneous Thermal Analysis (STA: TGA/DSC)

The used device STA 449 F3 Jupiter from Netzsch was equipped with a TGA/DSC measuring head. The measuring range was between 40 °C and 500 °C and the measuring rate was 1 K·min^{-1}. A gas flow of 100 mL·min^{-1} helium was set. All measurements were performed in Pt-crucibles without lids. Sample masses were 26 ± 2 mg for $[C_4C_1im]BF_4$ and 6 ± 1 mg for SeO_2 and 6 ± 1 mg for $Bi_2Se_3O_9$.

Evolved Gas Analysis (EGA) by Mass Spectrometry (TGA/DSC-MS)

The STA 449 F3 Jupiter from Netzsch was coupled by a transfer line to a QMS 403 D Aëolos mass spectrometer from Netzsch. The measurements were performed under a helium atmosphere with a gas flow of 100 mL·min^{-1}. The electron ionization energy was 70 eV and the mass range was between 1 and 300 amu. A temperature range from 40 °C to 500 °C with a heating rate of 1 K·min^{-1} was analyzed. Pt crucibles without lids were also used. To reduce capillary blockage at the inlet of the MS, the head temperature of the STA was lowered from 300 °C to 200 °C. The temperature of the transfer line and the inlet of the MS was adjusted to 300 °C. After initially a Bagraph (screening) measurement in the range $m/z = 0\ldots$ 300 was realized, a measurement with a new sample in MID mode was performed, in which the relevant species with characteristic mass numbers m/z identified by baraph measurement were

measured more precisely. The evaluation was performed using the implemented Proteus Analysis software by NETZSCH. Measurements at 35 eV were also performed but revealed no differences in the relevant *m/z*.

Evolved Gas AnalysisbBy Fourier Transform Infrared Spectrometry (TG-FTIR)

A TG 209 F1 Libra from Netzsch was coupled via transfer line with a Fourier Transform Infrared Spectrometer (FTIR) Vertrex 80v from BRUKER. The measurement was carried out in an argon atmosphere with a gas flow of 75 mL·min^{-1} in a temperature range from 40 °C to 300 °C at a heating rate of 1 K·min^{-1}. Platinum crucibles without lids were used and a sample quantity of 26 ± 2 mg for $[C_4C_1im]BF_4$ and 6 ± 1 mg for SeO_2 was weighed in. The head temperature of the TGA was 200 °C and the transfer line was tempered to 230 °C to prevent condensation of the gaseous species formed. The gas cell of the FTIR was heated to 200 °C. Spectra were recorded in a range from 4000 cm^{-1} to 600 cm^{-1}. The resolution was 2 cm^{-1} and 32 scans were taken for each spectrum. The evaluation was performed using Proteus and OPUS 8.1 software.

Characterization of the Solid

Photo Box

For the uniform optical recording of the vials during the reaction time of 3 h in the aluminum block, the samples were taken from the aluminum block and placed in a foldable photo box with a white or black background. For comparable display of the brightness of the samples, the integrated LED strip (5 V/1 A) with 34 LEDs was set to maximum brightness.

Light Microscopy

The solid material obtained in the vials during the synthesis process was microscopically examined after isolation using Stemi 2000-C from Zeiss. The images were documented by using the Motic Moticam 5 digital camera of the manufacturer CMOS-Sensor. Since agglomerates of the obtained solids showed an insufficient depth of focus, several images with different focus distances were taken and combined into one image using Helicon-Focus software. Thus, images with a better depth of focus could be created.

X-Ray Powder Diffraction (pXRD)

To characterize the phase purity of $Bi_2Se_3O_9$, as well as to identify the crystalline product samples formed after the DSC, STA, and vial experiments, X-ray diffractograms were taken. The diffractograms were recorded with the BRUKER D2 device at room temperature with an acceleration voltage of 30 kV and a filament current of 10 mA. The measurements were performed with CuKα radiation-λ = 154.056 pm (reflection mode) and nickel filter. The built-in detector is a LynxEye detector, which is a semiconductor strip detector system (192 strips = 3°(2θ)). The measuring range between 2θ was from 10° to 90°. A sample holder with silicon monocrystal was used for the measurement. After recording, the obtained diffractogram was examined for the contained phases using EVA software. Reference samples from the ICDD database were used for identification.

Scanning Electron Microscope (SEM)

A scanning electron microscope (SEM) XL30 ESEM LaB_6 from Philips was used to analyze the surface properties of the solid material obtained. The powder samples were scattered on a double-sided carbon tape which was glued to an aluminum stub. These were then sputtered with a gold film. The aluminum stub was placed in the vacuum chamber of the SEM. The sample was analyzed with a gas secondary electron detector (working pressure: 0.8 Torr, acceleration voltage: 30.00 kV). Energy dispersive X-ray (EDAX) microanalysis was performed using EDAX-DX4, which is built into the SEM. The energetic resolution was 10 eV and the detection limit was > 1 w%. The determination of the relative elemental composition was calculated directly with the EDAX software.

Acknowledgments

This work has been supported by the German Research Foundation (DFG) in the framework of the priority program SPP 1708 "Material Synthesis Near Room Temperature" (grant SCHM 1616/6-1,2). We also acknowledge the support by the European Regional Development Fund (ERDF-Brandenburg, project no. 85006795 and 80155970 see: www.efre.brandenburg.de). Additionally, we thank Prof. A. Kaiser and Dr. A. Efimova (both BTU Cottbus-Senftenberg, Faculty of Environment and Natural Sciences, Institute of Materials Chemistry) for helpful discussions. Finally, we acknowledge Tim Sieber (BTU Cottbus-Senftenberg) for experimental support performing the REM experiments and Maja Glorius (Dresden University of Technology, Faculty of Mechanical Engineering Institute of Power Engineering, Chair of Technical Thermodynamics) for the realization of the TGA-FTIR measurements. Open access funding enabled and organized by Projekt DEAL.

Conflict of Interest

The authors declare no conflict of interest.

Keywords: Bi_2Se_3 · ionic liquids · reaction mechanisms · selenium · time-dependent thermal decomposition

[1] P. Wasserscheid, T. Welton, *Ionic Liquids in Synthesis*, Wiley-VCH Verlag GmbH & Co. KGaA, Weinheim, Germany, **2007**.
[2] A. Thirumurugan, *Bull. Mater. Sci.* **2007**, *30*, 179.
[3] L. D. Pachón, G. Rothenberg, *Appl. Organomet. Chem.* **2008**, *22*, 288.
[4] D. Marquardt, J. Barthel, M. Braun, C. Ganter, C. Janiak, *CrystEngComm* **2012**, *14*, 7607.
[5] J. Krämer, E. Redel, R. Thomann, C. Janiak, *Organometallics* **2008**, *27*, 1976.
[6] Z. Li, Q. Yu, Y. Luan, G. Zhuang, R. Fan, R. Li, C. Wang, *CrystEngComm* **2009**, *11*, 2683.
[7] E. Redel, R. Thomann, C. Janiak, *Inorg. Chem.* **2008**, *47*, 14.
[8] P. Migowski, D. Zanchet, G. Machado, M. A. Gelesky, S. R. Teixeira, J. Dupont, *Phys. Chem. Chem. Phys.* **2010**, *12*, 6826.
[9] a) A. Taubert, R. Löbbicke, B. Kirchner, F. Leroux, *Beilstein J. Nanotechnol.* **2017**, *8*, 736; b) K. Zehbe, M. Kollosche, S. Lardong, A. Kelling, U. Schilde, A. Taubert, *Int. J. Mol. Sci.* **2016**, *17*, 391.
[10] Z. Ma, J. Yu, S. Dai, *Adv. Mater.* **2010**, *22*, 261.
[11] B. C. Leal, C. S. Consorti, G. Machado, J. Dupont, *Catal. Sci. Technol.* **2015**, *5*, 903.

[12] S. S. Mondal, D. Marquardt, C. Janiak, H.-J. Holdt, *Dalton Trans.* **2016**, *45*, 5476.
[13] a) A. A. Aal, R. Al-Salman, M. Al-Zoubi, N. Borissenko, F. Endres, O. Höfft, A. Prowald, S. Z. El Abedin, *Electrochim. Acta* **2011**, *56*, 10295; b) A. Abdel Aal, F. Voigts, D. Chakarov, F. Endres, *Electrochim. Acta* **2012**, *59*, 228; c) S. Z. El Abedin, A. Y. Saad, H. K. Farag, N. Borisenko, Q. X. Liu, F. Endres, *Electrochim. Acta* **2007**, *52*, 2746.
[14] a) J.-Y. Wan, Z. Yang, Z.-G. Liu, H.-X. Wang, *RSC Adv.* **2016**, *6*, 61292; b) E. Redel, R. Thomann, C. Janiak, *Chem. Commun.* **2008**, 1789.
[15] R. M. Esteban, H. Meyer, J. Kim, C. Gemel, R. A. Fischer, C. Janiak, *Eur. J. Inorg. Chem.* **2016**, 2106.
[16] K. Schütte, H. Meyer, C. Gemel, J. Barthel, R. A. Fischer, C. Janiak, *Nanoscale* **2014**, *6*, 3116.
[17] M. F. Groh, A. Wolff, M. A. Grasser, M. Ruck, *Int. J. Mol. Sci.* **2016**, *17*, 1452.
[18] A. Efimova, L. Pfützner, P. Schmidt, *Thermochim. Acta* **2015**, *604*, 129.
[19] A. Efimova, J. Varga, G. Matuschek, M. R. Saraji-Bozorgzad, T. Denner, R. Zimmermann, P. Schmidt, *J. Phys. Chem. B* **2018**, *122*, 8738.
[20] A. Seeberger, A.-K. Andresen, A. Jess, *Phys. Chem. Chem. Phys.* **2009**, *11*, 9375.
[21] M. Knorr, M. Icker, A. Efimova, P. Schmidt, *Thermochim. Acta* **2020**, 178786.
[22] Y.-J. Zhu, W.-W. Wang, R.-J. Qi, X.-L. Hu, *Angew. Chem.* **2004**, *116*, 1434.
[23] a) J. Ma, J. Lian, X. Duan, Z. Liu, P. Peng, X. Liu, T. Kim, W. Zheng, *CrystEngComm* **2011**, *13*, 2774; b) Y. Jiang, Y.-J. Zhu, *J. Phys. Chem. B* **2005**, *109*, 4361; c) Y. Jiang, Y.-J. Zhu, *J. Cryst. Growth* **2007**, *306*, 351.
[24] Y. Jiang, Y.-J. Zhu, G.-F. Cheng, *Cryst. Growth Des.* **2006**, *6*, 2174.
[25] P. S. Reddy, S. Kanjilal, S. Sunitha, R. B. N. Prasad, *Tetrahedron Lett.* **2007**, *48*, 8807.
[26] a) C. Agapescu, A. Cojocaru, F. Golgovici, A. C. Manea, A. Cotarta, *Rev. Chim. (Bucharest)* **2012**, *63*, 911; b) A. C. Cojocaru, M. Sima, *Rev. Chim. (Bucharest)* **2012**, 217; c) M. Steichen, P. Dale, *Electrochem. Commun.* **2011**, *13*, 865.
[27] H. Oppermann, H. Gbel, H. Schadow, V. Vassilev, I. Markova-Deneva, *Z. Anorg. Allg. Chem.* **1996**, *622*, 2115.
[28] H. Oppermann, H. Göbel, H. Schadow, P. Schmidt, C. Hennig, V. Vassilev, I. Markova-Deneva, *Z. Naturforsch. B* **1999**, *54*, 239.
[29] a) J. D. Holbrey, K. R. Seddon, *J. Chem. Soc. Dalton Trans.* **1999**, 2133; b) M. E. V. Valkenburg, R. L. Vaughn, M. Williams, J. S. Wilkes, *Thermochim. Acta* **2005**, *425*, 181; c) C. P. Fredlake, J. M. Crosthwaite, D. G. Hert, A. Sudhir, N. V. K. J. F. Brennecke, *J. Chem. Eng. Data* **2004**, *49*, 954; d) J. G. Huddleston, A. E. Visser, W. M. Reichert, H. D. Willauer, G. A. Broker, R. D. Rogers, *Green Chem.* **2001**, *3*, 156; e) T. Erdmenger, J. Vitz, F. Wiesbrock, U. S. Schubert, *J. Mater. Chem.* **2008**, *18*, 5267.
[30] a) I. Paramasivam, J. M. Macak, T. Selvam, P. Schmuki, *Electrochim. Acta* **2008**, *54*, 643; b) Z. Li, Z. Du, Y. Gu, L. Zhu, X. Zhang, Y. Deng, *Electrochem. Commun.* **2006**, *8*, 1270.
[31] O. Knacke, O. Kubaschewski, K. Hesselmann, *Thermochemical properties of inorganic substances*, Springer-Verlag, Berlin, Heidelberg, **1991**
[32] P. Linstrom, *NIST Chemistry WebBook, NIST Standard Reference Database 69*, National Institute of Standards and Technology, **1997**
[33] K. J. R. Rosman, P. D. P. Taylor, *Pure Appl. Chem.* **1998**, *70*, 217.
[34] J. R. Durig, T. S. Little, *J. Chem. Phys.* **1981**, *75*, 3660.
[35] H. L. Riley, J. F. Morley, N. A. C. Friend, *J. Chem. Soc.* **1932**, 1875.
[36] H. L. Riley, N. A. C. Friend, *J. Chem. Soc.* **1932**, 2342.
[37] J. Clayden, S. Warren, N. Greeves, P. Wothers, *Organic chemistry*, Oxford University Press, New York, **2007**
[38] K. B. Sharpless, R. F. Lauer, *J. Am. Chem. Soc.* **1972**, *94*, 7154.
[39] a) L. M. Stephenson, D. R. Speth, *J. Org. Chem.* **1979**, *44*, 4683; b) D. A. Singleton, C. Hang, *J. Org. Chem.* **2000**, *65*, 7554.
[40] H. Gobrecht, G. Willers, D. Wobig, *J. Phys. Chem. Solids* **1970**, *31*, 2145.
[41] R. Böhmer, C. A. Angell, *Phys. Rev. B* **1993**, *48*, 5857.
[42] A. J. Bradley, *Philos. Mag.* **1924**, *48*, 477.
[43] C. P. Shah, C. Dwivedi, K. K. Singh, M. Kumar, P. N. Bajaj, *Mater. Res. Bull.* **2010**, *45*, 1213.
[44] A. P. Saunders, *J. Phys. Chem.* **1899**, *4*, 423.
[45] a) J. Zhang, Z. Peng, A. Soni, Y. Zhao, Y. Xiong, B. Peng, J. Wang, M. S. Dresselhaus, Q. Xiong, *Nano Lett.* **2011**, *11*, 2407; b) W. Zhang, R. Yu, H.-J. Zhang, X. Dai, Z. Fang, *New J. Phys.* **2010**, *12*, 65013; c) G. L. Sun, L. L. Li, X. Y. Qin, D. Li, T. H. Zou, H. X. Xin, B. J. Ren, J. Zhang, Y. Y. Li, X. J. Li, *Appl. Phys. Lett.* **2015**, *106*, 53102

Manuscript received: September 4, 2020
Revised manuscript received: November 6, 2020